Journal of Molecular Structure 985 (2011) 139–147

Contents lists available at ScienceDirect

Journal of Molecular Structure

journal homepage: www.elsevier.com/locate/molstruc

Molecular structure and vibrational assignments of bis(4-aminopent-3-en-2-onato)copper(II): A detailed density functional theoretical study

Mina Jamialahmadi [a], Sayyed Faramarz Tayyari [a,*], Mohammad Hossein Habibi [b], Mohammad Yazdanbakhsh [a], Saeideh Kadkhodaei [a], Robert Erik Sammelson [c]

[a] Department of Chemistry, Ferdowsi University of Mashhad, Mashhad 91775-1436, Iran
[b] Department of Chemistry, University of Isfahan, Isfahan 81746-73441, Iran
[c] Department of Chemistry, Ball State University, Muncie, IN 47306-0445, USA

ARTICLE INFO

Article history:
Received 27 August 2010
Received in revised form 21 October 2010
Accepted 21 October 2010
Available online 3 November 2010

Keywords:
Bis(4-aminopent-3-en-2-onato)copper(II)
X-ray crystallography
Density functional theory
FT-IR spectroscopy
FT-Raman Spectroscopy

ABSTRACT

Bis(4-aminopent-3-en-2-onato) copper(II), $Cu(APO)_2$, was synthesized and its total X-ray crystallographic data were determined. The molecular structure and vibrational spectra of this compound were investigated by means of density functional theory (DFT) calculations at the B3LYP level using 6-31G**, 6-311G*, and 6-31++G* basis sets, and the results were compared with the experimental data. For comparison, the geometrical parameters and vibrational wavenumbers of $Cu(APO)_2$ were also calculated at the HF and MPW1PW91 levels using mixed basis sets (GEN), 6-311+G* for the Cu atom and 6-31G** for all the other atoms. All of the measured IR and Raman bands were interpreted in terms of the calculated vibrational modes. The scaled theoretical frequencies and the structural parameters were in good agreement with the experimental data.

© 2010 Elsevier B.V. All rights reserved.

1. Introduction

The late transition metals can be stabilized by heterodonor ligands with multiple coordination modes and give mono- and dinuclear complexes. In particular, these ligands are very important for the development of transition metal complexes with O and N mixed ligands [1,2]. Therefore, complexes containing ligands of the N,O-chelate family could be of particular interest. β-ketoamines are important members of this general family because of their ease of preparation and modification of both steric and/or electronic effects. These compounds are versatile synthetic intermediates that combine the ambident nucleophilicity of enamines with the ambident electrophilicity of enones and have been extensively used for the preparation of a variety of heterocyclic systems including some natural products and their analogues [3,4].

During recent years the use of late transition metal catalysts has been extensively studied [5]. Bao et al. [6] have investigated a series of copper(II) complexes of β-ketoamine ligands for polymerization of olefins.

Gurr [7] has studied the structure of bis(4-aminopent-3-en-2-onato)copper(II) by X-ray crystallographic diffraction method. According to the results of Gurr, $Cu(APO)_2$ is orthorhombic with a unit cell dimensions of 16.9 × 15.2 × 13.8 Å. It is also shown that the single molecule of this compound, cannot have 222-point symmetry, which indicates that the molecules at these sites are disordered, having at random either one of two following orientations given in Scheme 1.

Therefore, the average of these two structures has 222-point symmetry about the metal atom.

The aim of the present work is the modified synthesis, the improved understanding of the structural information, and the full assignment of the vibrational spectra (harmonic wavenumbers, and relative intensities for Raman and IR spectra) of $Cu(APO)_2$ by means of density functional theory (DFT) studies. The calculated vibrational frequencies are compared with those observed experimentally.

2. Experimental

2.1. Synthesis

$Cu(APO)_2$ was synthesized according to Lacey [8] with minor changes (using concentrated ammonia (25%) and a solution of copper acetate in absolute ethanol and ammonia). After recrystallization from ethanol, the needle like crystals obtained, m.p. 195 °C (yield 62%). Anal. Calc. for $CuC_{10}H_{16}O_2N_2$: C, 46.23; H, 6.21; N,

* Corresponding author. Tel.: +98 511 8780216; fax: +98 511 8438032.
E-mail address: Tayyari@ferdowsi.um.ac.ir (S.F. Tayyari).

0022-2860/$ - see front matter © 2010 Elsevier B.V. All rights reserved.
doi:10.1016/j.molstruc.2010.10.034

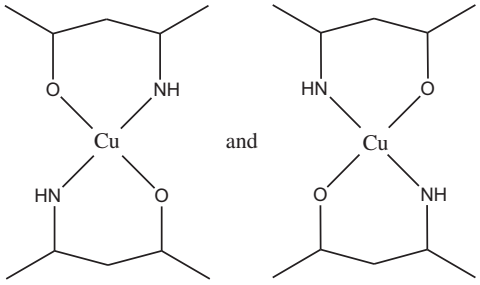

Scheme 1.

10.78. Found: C, 46.86; H, 6.26; N, 10.52%. Single crystals of Cu-$(APO)_2$ were obtained from a CH_3OH/C_2H_5OH(1:1) solution by slow evaporation at room temperature.

2.2. Instrumentation

The IR spectra were recorded on a Bomem B-154 Fourier Transform spectrophotometer in the region 4000–600 cm^{-1} by averaging 20 scans with a resolution of 2 cm^{-1}. The spectra were measured as KBr pellets and in CH_3CN, $CHCl_3$, and CCl_4 solution.

The Far-IR spectra in the 600–100 cm^{-1} region were obtained using a Thermo Nicolet NEXUS 870 FT-IR spectrometer equipped with a DTGS/polyethylene detector and a solid substrate beam splitter. The spectrum of the polyethylene pellet was collected with a resolution of 2 cm^{-1} by averaging the results of 64 scans.

The FT-Raman spectra were recorded employing a 180° back scattering geometry and a Bomem MB-154 Fourier transform Raman spectrometer. The instrument was equipped with a Nd: YAG laser beam source (λ = 1064 nm), ZnSe beam splitter, and a TE cooled InGaAs detector. Rayleigh filtration was afforded by two sets of two holographic technology filters. The spectra were accumulated for 500 scans with a resolution of 2 cm^{-1}. The laser power at the sample was 400 mW.

2.3. Single crystal X-ray measurements

X-ray data of $Cu(APO)_2$ were collected on a Rigaku RAXIS RAPID imaging plate area detector with graphite monochromated Mo Kα radiation (λ = 0.71075 Å). Indexing was performed from 3 oscillations that were exposed for 150 s. The crystal-to-detector distance was 127.40 mm.

The structure was solved by heavy-atom Patterson methods [9] and expanded using Fourier techniques [10]. The non-hydrogen atoms were refined anisotropically. Hydrogen atoms were refined using the riding model. The final cycle of full-matrix least-squares refinement on F^2 was based on 1956 observed reflections and 135 variable parameters and converged with unweighted and weighted agreement factors of:

$$R_1 = \sum[|F_o| - |F_c|] \Big/ \sum |F_o| = 0.0429$$

$$wR_2 = \left[\sum \left(w\left(F_o^2 - F_c^2\right)^2 \Big/ \sum w\left(F_o^2\right)^2\right]^{1/2} = 0.1152$$

The standard deviation of an observation of unit weight was 1.11. Unit weights were used. The maximum and minimum peaks on the final difference Fourier map corresponded to 0.41 and −0.42 e-/Å^3, respectively.

3. Method of analysis

In this study, the molecular equilibrium geometry, harmonic force field, and vibrational transitions of $Cu(APO)_2$ were computed with the GAUSSIAN 03W software system [11].

It has been shown that for obtaining the vibrational frequencies of β-diketone metal complexes the B3LYP level [12,13] gives superior results [14]. Therefore, the B3LYP level, using 6-31G*, 6-31++G*, and 6-311G* basis sets, have been utilized for optimization and vibrational frequency calculations. In addition, it was also shown that the MPW1PW91 level gives remarkable results both for covalent and non-covalent interactions [15], therefore, the calculations were also performed at the MPW1PW91, using mixed basis sets, 6-311+G* basis set for Cu atom and 6-31G** for the others (GEN). For comparison, the calculations were also repeated at the HF level, using the same mixed basis sets.

Raman activities were computed by numerical differentiation of dipole derivatives with respect to the electric field, using standard GAUSSIAN 03 procedures (Freq = Raman) and default options.

The assignment of the experimental frequencies were based on the observed band frequencies and intensities in the infrared and Raman spectra confirmed by establishing one to one correlation between observed and theoretically calculated frequencies. The assignment of the calculated wavenumbers was aided by the animation option of the GaussView 4.1 graphical interface for Gaussian programs [16], which gives a visual representation of the shape of the vibrational modes.

Lorentzian function has been utilized for deconvolution of all IR and Raman spectra using Genplot package [17].

4. Results and discussion

The crystallographic data and the details of the X-ray analysis are represented in Table 1.

As it is shown in Table 1, the obtained unit cell dimensions (16.9 × 15.0 × 13.6 Å) are slightly different from that reported by Gurr [7]. Selected bond lengths and angles for this compound are given in Table 2, and the calculated and X-ray geometry for Cu(A-PO)$_2$ are shown in Figs. 1 and 2, respectively.

Table 1
Crystallographic data for bis(4-amino-3-penten-2-ono)copper(II).

Empirical formula	$CuC_{10}H_{16}O_2N_2$
Formula weight	259.79
Temperature (K)	188
Wavelength (Å)	0.71075
Crystal system, space group	Orthorhombic
Unit cell dimensions	
a (Å)	15.0102(17)
b (Å)	16.8904(18)
c (Å)	13.5844(13)
V (Å^3)	3444.0(6)
Z, calculated density (g cm^{-3})	12, 1.503
Absorption coefficient (cm^{-1})	18.849
F(000)	1620.00
Crystal size (mm)	0.50 × 0.30 × 0.30
ω Oscillation range (χ = 45.0, φ = 0.0)	130.0–190.0°
Exposure rate (s/°)	200.0
ω Oscillation range (χ = 45.0, φ = 180.0)	130.0–190.0°
Exposure rate (s/°)	200.0
Detector position (mm)	127.40
Pixel size (mm)	0.100
$2\theta_{max}$	54.8°
Reflections collected/unique [R(int)]	15989/1956 (0.034)
Corrections	Lorentz-polarization Absorption (trans. factors: 0.416–0.568)
Refinement	Full-matrix least-squares on F^2
Function Minimized	$\Sigma w(F_o^2 - F_c^2)^2$
R indices (all data)	R_1 = 0.0429 wR_2 = 0.1152
Max. and min. transmission	0.41 and −0.42
Goodness-of-fit on F^2	1.113

Table 2
Selected experimental (X-ray) and calculated geometrical parameters for bis(4-amino-3-penten-2-ono)copper(II).[a]

	X-ray	UHF	UB3LYP			UMPW1PW91	APO[b]
		GEN	6-31G*	6-31++G*	6-311G*	GEN	
Bond lengths							
Cu_2–O_2	1.958(14)	1.969	1.925	1.968	1.955	1.951	
Cu_2–N_2	1.89(2)	1.987	1.912	1.930	1.920	1.917	
O_1–C_2	1.393(14)	1.264	1.287	1.288	1.280	1.281	1.253
N_1–C_2	1.19(2)	1.294	1.315	1.314	1.309	1.308	1.349
C_2–C_3	1.393(3)	1.382	1.394	1.395	1.392	1.389	1.443
C_3–C_4	1.393(3)	1.419	1.417	1.420	1.418	1.414	1.379
C_1–C_2	1.507(5)	1.512	1.516	1.517	1.514	1.508	1.507
N_2–H_2	0.880	0.999	1.017	1.017	1.013	1.013	1.021
C_1–H_1	0.980	1.084	1.084	1.085	1.083	1.083	
Bond angles							
O_1–Cu_1–O_1	177.0(5)	179.99	160.47	179.97	179.78	179.99	
O_1–Cu_1–N_1	92.0(8)	90.39	92.50	91.58	88.51	88.22	
N_2–Cu_2–N_3	174.0(10)	179.99	161.18	179.96	179.77	179.99	
Cu_1–O_1–C_2	125.6(12)	128.53	126.66	126.54	126.82	126.44	
Cu_1–N_1–C_2	126.6(15)	127.84	128.20	128.65	128.71	128.50	
O_1–C_2–C_3	122.5(8)	125.90	125.68	125.67	125.76	125.99	123.4
N_1–C_2–C_3	125.2(11)	123.85	122.52	122.78	122.88	122.96	121.3
C_7–C_8–C_9	125.5(3)	124.28	124.36	124.77	124.32	124.34	122.7
Cu_1–N_1–H_1	116.7	117.97	117.08	116.07	116.02	116.47	
C_2–N_1–H_1	116.7	114.19	114.39	115.27	115.27	115.02	116.1
C_2–C_1–H_1	109.5	109.89	111.45	111.68	111.84	111.82	
H_1–C_1–H_1	109.5	108.78	108.04	108.38	108.18	108.55	
ΔE (kJ/mol)			10.654	22.773	24.130		

[a] Bond lengths in Å, bond angles in °; $\Delta E = E(\text{cis}) - E(\text{trans})$.
[b] Data from Ref. [13].

4.1. Molecular geometry

Two configurations, cis and trans, are possible for the $Cu(APO)_2$ complex (Fig. 1). According to the theoretical DFT calculations, the trans configuration proved more stable than the cis configuration for all levels and basis sets, which is in agreement with the Gurr's results [7]. According to the crystallographic results, Fig. 2, the complex molecules are randomly lay in the unit cells, but in all arrangements the complex has only trans configuration. However, as it is shown in Table 2, the most geometrical parameters for all of theoretical levels are in excellent agreement with the experimental results. Due to of the special structure of the single crystal of $Cu(APO)_2$, some of the experimental X-ray results (for example C—O and C—N bond lengths) are somewhat different from the theoretical ones. The best agreement between theoretical and experimental data were obtained by using UMPW1PW91/GEN and UB3LYP/6-311G* levels.

As it is shown in Table 2, the calculated C—O and C_3—C_4 bond lengths were longer and the C—N and C_2—C_3 bond lengths were shorter than the corresponding values in APO [18]. These results suggests that the π-delocalization in the chelated ring of $Cu(APO)_2$ is increased relative to APO.

N—H and C—H_α bond lengths are longer than the same values in X-ray. This is a well known phenomenon that the X-ray diffraction cannot measure the bond lengths including H atom and an electronegative element such as O or N, precisely. The main reason for this disability is that the electron cloud is stretched toward electronegative atom and because diffraction is done by electrons, to specify the exact position of the nucleus is impossible. This causes the measured length of such bonds to be shorter in X-ray spectroscopy.

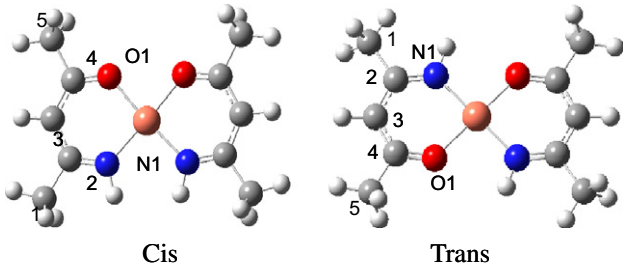

Fig. 1. Cis and trans configurations of $Cu(APO)_2$, optimized by 6-311G* basis set and atom numbering system.

4.2. Vibrational analysis

The fundamental wavenumbers obtained with different levels and basis sets were compared with the experimental ones by means of regression analysis separately for both 1700–3100 and 50–1700 cm^{-1} region. Simple scaling of the theoretical wavenumbers according to the equation $\nu_{OBSD} = \alpha\nu_{THEOR}$ generally leads to satisfactory agreement with the set of the observed wavenumbers; the least-square scaling factors α, regression coefficients R^2, and standard deviations (SD) are listed in Table 3 for both the high and low frequency regions. The best values for scaling factors have been obtained by UB3LYP/6-311G* level and basis set. In this work, 0.9604 and 0.9832 scaling factors have been used for high and low frequencies, respectively. The calculated values for α are in excellent agreement with those reported in Ref. [14].

The infrared spectra of $Cu(APO)_2$ in the 3400–2800 and 1700–500 cm^{-1} regions are shown in Figs. 3 and 4, respectively. Figs. 5 and 6 represent the Raman and far infrared spectra of this compound. Lorentzian function has been utilized for deconvolution of the IR spectra and deconvoluted spectrum from 1650 to 1320 cm^{-1} is shown in Fig. 7. The theoretical and experimental IR and Raman band frequencies in the solid phase and solutions for trans configuration and their assignments are given in Table 4.

The fundamental wavenumbers calculated at the different DFT levels are compared with the experimental results. The calculated frequencies are slightly higher than the observed values for the majority of the normal modes. Two factors may be responsible for the discrepancies between the experimental and computed spectra of $Cu(APO)_2$. The first is caused by the environment. DFT calculations have been done at the gas phase, and experimental

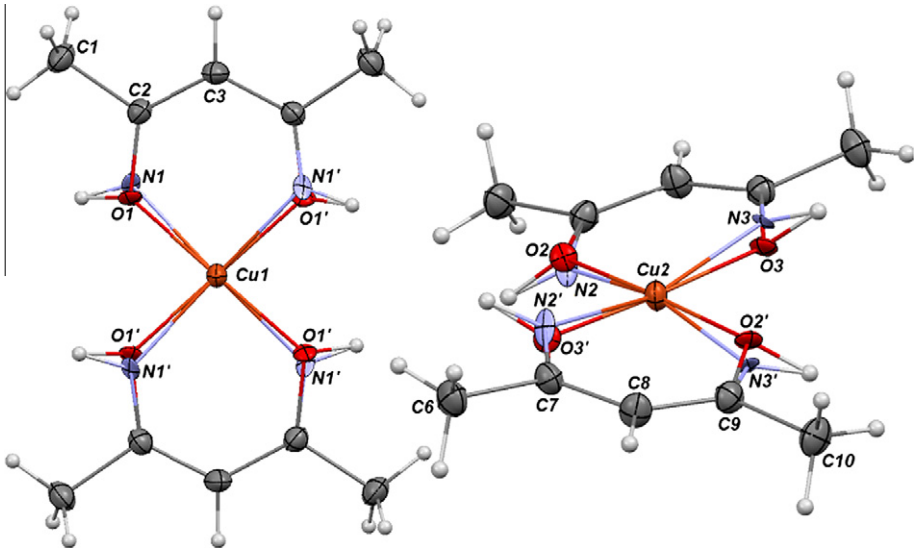

Fig. 2. ORTEP structure of $Cu(APO)_2$ showing the thermal ellipsoids at 50% probability.

Table 3
$Cu(APO)_2$ scaling factors α, regression coefficients R^2, and standard deviations SD (cm^{-1}) for regressions of observed vibrational wavenumbers on theoretical ones (see text)[a].

	Regression, high frequency			Regression, low frequency		
	α	R^2	SD	α	R^2	SD
UB3LYP/6-31G*	0.9543	0.999994	9.2	0.9772	0.999951	9.2
UB3LYP/6-31++G*	0.9560	0.999996	7.4	0.9839	0.999947	9.5
UB3LYP/6-311G*	0.9604	0.999997	6.0	0.9832	0.999948	9.4
UHF/GEN	0.9112	0.999996	11.5	0.9106	0.999733	21.4
UMPW1PW91/GEN	0.9432	0.999975	18.0	0.9747	0.999743	21.0

[a] 6-311+G* basis set for Cu atom and 6-31G** for other atoms.

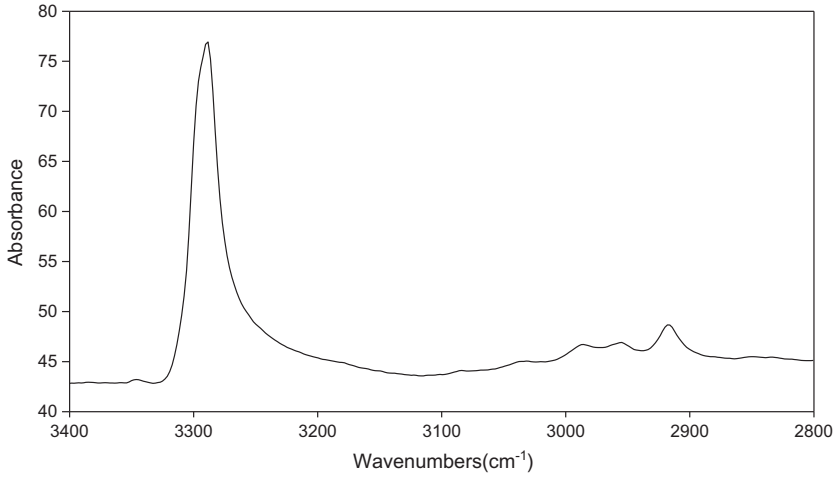

Fig. 3. Infrared spectrum of $Cu(APO)_2$ in the solid phase, in the 3400–2800 cm^{-1} region.

data are obtained at condensed phases. The second reason for this discrepancy is the fact that the experimental values are anharmonic frequencies, while the calculated values are harmonic frequencies.

4.2.1. 3500–1700 cm^{-1} region

In this region C—H and N—H stretching modes are expected to be observed. The N—H stretching of primary amines occurs at 3380–3350 and 3310–3280 cm^{-1} for symmetric and asymmetric stretching vibrations, respectively [19]. In the case of secondary amines the N-H stretching falls in the 3320–3280 cm^{-1} region [19]. However, the existence of intramolecular hydrogen bond perturbs this pattern [18]. Since our calculations have been done in the gas phase without considering the formation of hydrogen bonds, the theoretical N—H stretching bands have appeared at much higher frequencies than that observed experimentally. In the infrared spectrum of $Cu(APO)_2$ in the solid phase one strong band is observed at about 3290 cm^{-1}, which shifts to 3334, 3351, and 3356 cm^{-1} in the CH_3CN, $CHCl_3$, and CCl_4 solutions, respectively (Fig. 8). According to the theoretical calculations and

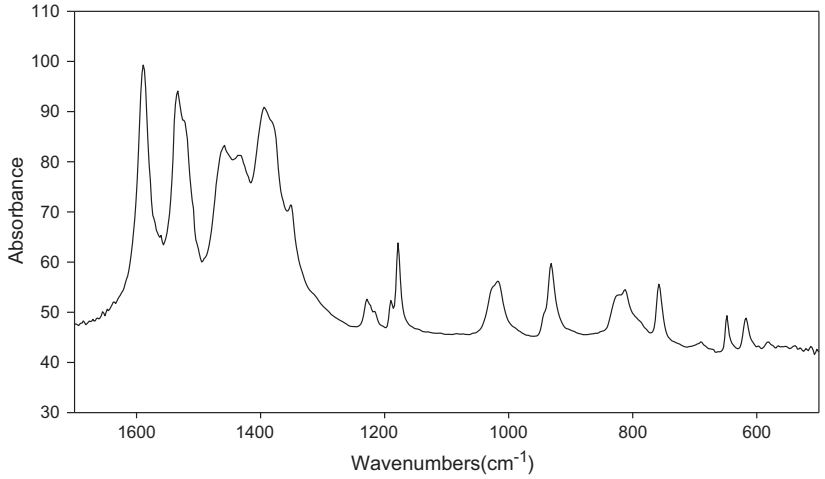

Fig. 4. Infrared spectrum of $Cu(APO)_2$ in the solid phase, in the 1700–500 cm^{-1} region.

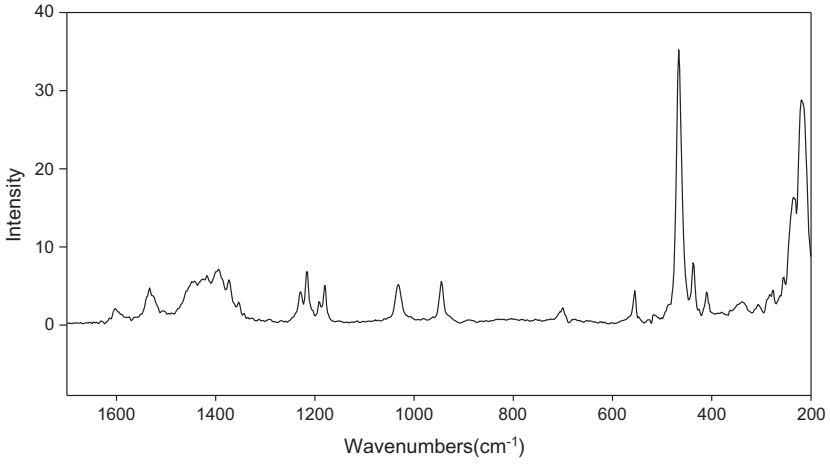

Fig. 5. Raman spectrum of $Cu(APO)_2$ in the solid phase.

considering the above discussion, we assigned this band to the N—H stretching mode. These results suggest that in solution, the intermolecular hydrogen bond becomes weaker than in the solid phase. Therefore, the N—H stretching band shifts towards higher frequencies in solution. By comparing the N—H frequencies in the CCl_4 and CH_3CN solutions, one may conclude that there is a weak intermolecular hydrogen bond formation between the N—H group and CH_3CN solvent molecules. The 3083 cm^{-1} band in the Raman and IR spectra of $Cu(APO)_2$ in the solid phase is assigned to the CH_α stretching mode. The corresponding band in AA is reported to be occurred at 3090 cm^{-1} [24]. The CH stretching modes of the CH_3 groups in acetylacetone, AA, and its metal complexes are reported to occur in the 3000–2900 cm^{-1} region [14,20–24]. Two bands are observed in the Raman spectrum at 2986 and 2914 cm^{-1}. The latter band is strong and the former has weak scattering intensity in the Raman spectrum. These two bands are assigned to the asymmetric and symmetric CH stretching modes of the CH_3 groups, respectively.

4.2.2. 1700–1000 cm^{-1} region

This was deemed the most significant region of the spectra. Beside the CH_3 and NH deformation and rocking, C—CH_3 stretching and CH in-plane bending modes, four bands are expected to be observed in this region in relation to the chelate ring modes which are attributed to the C⋯*O*, C—C, C⋯*C*, and C⋯*N* stretching modes. There is excellent agreement between theoretical and experimental results in this region. The strong IR band at 1590 cm^{-1} assigned to the out-of-phase C⋯*O* and C⋯*N* stretching. This band has been assigned by Holtzclaw et al. [25] to the C⋯*C* stretching. Deconvoluted IR spectrum of $Cu(APO)_2$ in $CHCl_3$ indicate the presence of two bands at about 1530 and 1517 cm^{-1}. In the solid phase these bands were observed at slightly higher frequencies. According to the calculation results, the former is assigned to the N—H in-plane bending, which is strongly coupled to the C—H in-plane bending and C⋯*C*⋯*C* asymmetric stretching vibrations. The 1517 cm^{-1} band is resulted from asymmetric C⋯*C*⋯*O* and C⋯*C*⋯*N* stretching vibrations. Holtzclaw et al. assigned the 1530 cm^{-1} band to the C═C or C═N stretching and did not observed the 1517 cm^{-1} band [25]. The bands at 1460, 1455, and 1396 cm^{-1} are attributed to the CH_3 deformation modes.

The 1435 cm^{-1} band in the IR spectrum of the solid phase is assigned to the in-plane asymmetric C⋯*C*⋯*O* and C⋯*C*⋯*N* stretching vibrations, which is coupled to the CH_3 deformation. This band is phase sensitive and its corresponding Raman band observed at 1422 cm^{-1}.

The IR band at 1180 cm^{-1} is assigned to the CH_α in-plane bending mode which is somewhat coupled to the N—H in-plane bending and C—CH_3 stretching movements. The corresponding band in

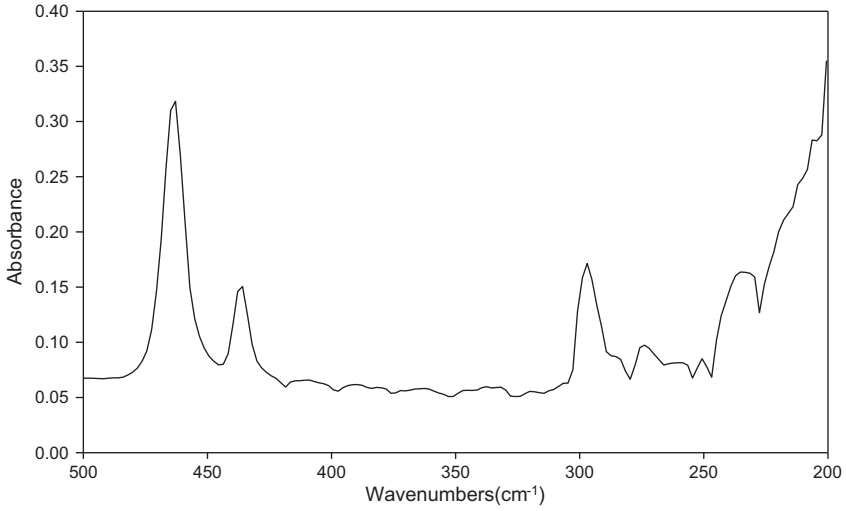

Fig. 6. Far Infrared spectrum of $Cu(APO)_2$ in the solid phase.

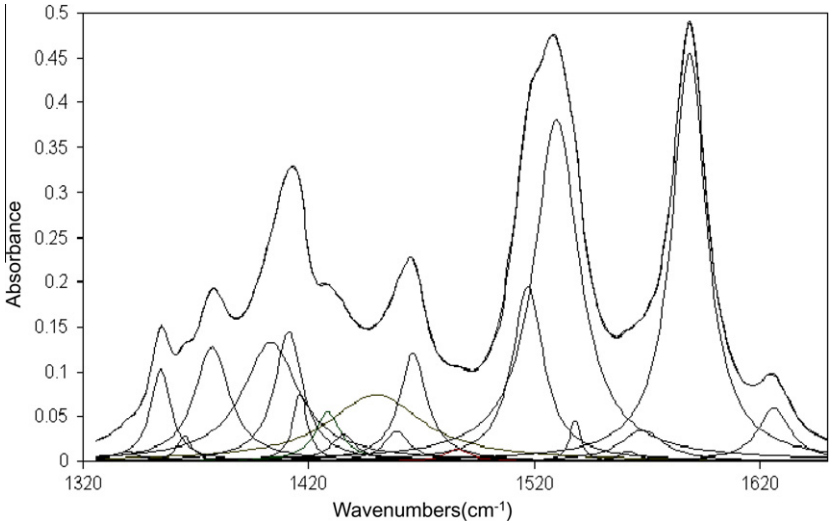

Fig. 7. The deconvoluted IR spectrum of Cu $(APO)_2$ in $CHCl_3$ solution, in the 1650–1320 cm^{-1} region.

acetylacetone, AA, [25], magnesium acetylacetonate, $Mg(acac)_2$, [14], and beryllium acetylacetonate, $Be(acac)_2$, [21] were observed at 1173, 1198, and 1191 cm^{-1}, respectively.

The band at 1017 cm^{-1} is assigned to CH_3 rocking coupled with in-plane ring deformation.

4.2.3. Below 1000 cm^{-1}

In this region one expects to observe C—CH_3 stretching, N—H, C—H out-of-plane bending modes, and in-plane and out-of-plane ring deformations.

The infrared spectrum in the solid phase shows a weak band at 787 cm^{-1}. According to the theoretical calculations this band is assigned to the C—H out-of-plane bending which is coupled with the N—H out-of-plane bending. The corresponding vibrational mode in AA [25], $Mg(acac)_3$ [14], and $Be(acac)_2$ [21] were observed at 785, 788, and 781 cm^{-1}, respectively.

The IR band at 621 cm^{-1}, according to the calculated results, is attributed to the asymmetric O—Cu—O and N—Cu—N stretching movements. The corresponding band in $Cu(acac)_2$ is reported to be occurred at 614 cm^{-1} [26].

The very strong far infrared band at 464 cm^{-1} and the Raman band at 466 cm^{-1} are assigned to the asymmetric and symmetric O—Cu—O stretching (coupled to N—Cu—N stretching), respectively. The latter does not include any movement of the metal; and therefore, this frequency may be useful in estimation of the metal–oxygen/nitrogen bond strength in the ketoamine complexes. The corresponding band in $Be(acac)_2$ [21], $Mg(acac)_2$ [14], and $Cu(acac)_2$ [26] were observed at 480, 414, and 455 cm^{-1}, respectively.

The relatively strong IR band at 297 cm^{-1} is assigned to the O–Cu–O and N–Cu–N in-plane bending vibration. The corresponding band in the IR spectrum of $Cu(acac)_2$at 291 cm^{-1} is assigned by Mikami et al. [27] and Nakamoto et al. [28] to the Cu—O stretching.

5. Conclusion

Infrared, Raman and far-IR spectra of $Cu(APO)_2$ were recorded both in crystalline and in solutions. The molecular and crystal structures were determined by single crystal X-ray diffraction. The structural parameters and vibrational frequencies of $Cu(APO)_2$ were calculated at the DFT level. Comparison between experimental and theoretical results was satisfactory. However, because of the special structure of the single crystal of $Cu(APO)_2$, the observed C—O and C—N bond lengths were somewhat deviated from the

Table 4
Fundamental band assignment of $Cu(APO)_2$.

Theoretical				Experimenta					Assignment
				IR				Raman	
No.	F_s	I_{IR}	A_R	Solid	CH_3CN	$CHCl_3$	CCl_4	Solid	
1	3412	21	25	3294(s)	3352(w)	3351(m)	3356(m)		νN—H
2	3412	4	125	3289(s)	3334(m)				νN—H
3	3066	12	140	3041(w)				3043(w)	νCH_α
4	3065	25	66	3041(w)				3043(w)	νCH_α
5	2998	30	78	2986(w)	2990(w)	(*)	2990(w)	2986(s)	νaCH_3
6	2998	25	93	2986(w)	2990(w)	(*)	2990(w)	2986(s)	νaCH_3
7	2991	32	49	2986(w)	2990(w)	(*)	2990(w)	2986(s)	νaCH_3
8	2991	13	90	2986(w)	2990(w)	(*)	2990(w)	2986(s)	νaCH_3
9	2973	18	72						νaCH_3
10	2973	13	104						νaCH_3
11	2969	35	6	2956(w)	2965(w)	2963(w)	2963(w)		νaCH_3
12	2969	1	193						νaCH_3
13	2918	10	309	2917(w)	2928(m)	2923(m)	2923(m)	2914(m)	νsCH_3
14	2918	18	195	2917(w)	2928(m)	2923(m)	2923(m)	2914(m)	νsCH_3
15	2917	2	279	2917(w)	2928(m)	2923(m)	2923(m)	2914(m)	νsCH_3
16	2917	47	14	2917	2928(m)	2923(m)	2923(m)	2914(m)	νsCH_3
17	1623	0	5			1626(vw)		1603(w)	$\nu C\cdots O$, $\nu C\cdots N$ (i.p.)
18	1611	610	0	1590(vs)	1590(vs)	1589(vs)	1589(vs)		$\nu C\cdots O$, $\nu C\cdots N$ (o.p.)
19	1542	0	8					1534(m)	δNH, δCH_α, νa C$\cdots$C$\cdots$C
20	1541	506	0	1535(vs)	1528(vs)	1530(vs)	1533(vs)		δCH_α, δNH, νa C$\cdots$C$\cdots$C
21	1510	320	0	1521(s)		1517(s)	1514(s)		$\nu aC\cdots C\cdots N$, $\nu aC\cdots C\cdots O$, δCH_3
22	1496	0	17						$\nu aC\cdots C\cdots N$, $\nu aC\cdots C\cdots O$, δCH_3
23	1479	40	10	1460(s)		1466(m)	1465(m)		δCH_3
24	1479	56	10	1460		1466	1465		δCH_3
25	1468	9	9	1460		1466	1465		δCH_3
26	1467	83	16	1455(sh)	*	1466	1465	1457(sh)	δCH_3
27	1466	5	22					1457	δCH_3
28	1466	21	1	1455			1458(m)		δCH_3
29	1455	363	1	1435(m)		1412(s)	1412(s)		δsCH_3, νaC=C=N, νaC=C=O
30	1438	0	22					1422(m)	δsCH_3, νaC=C=N, νaC=C=O
31	1398	0	40					1395(m)	δCH_3, νC—CH_3, δN—H
32	1396	32	1	1396(s)	*	1403(m)	1391(w)		δCH_3
33	1392	0	29					1395	δCH_3, δN—H
34	1390	24	0	1396		1403	1391		δCH_3, δN—H
35	1382	0	9					1373(m)	δCH_α, δNH, δsCH_3
36	1375	140	0	1378(m)	*	1377(s)	1375(m)		δNH, δCH_α, δC=C=C, δCH_3
37	1232	15	0	1229(m)					δCH_α, δNH, νsO=C—C, νC—CH_3
38	1221	0	32					1214(m)	δCH_α δNH, νO=C, νC—CH_3
39	1181	51	0	1180(m)	1173(w)	1171(m)	1169(w)		δCH_α, δNH, νaC—C—CH_3
40	1176	0	15					1178(m)	δCH_α, δNH, νsC—C—CH_3
41	1046	0	1						πCH_3
42	1046	1	0						πCH_3
43	1038	31	0						πCH_3
44	1037	1	0	1034(w)					πCH_3
45	1032	0	11					1027.0	ρCH_3, δC—C—C
46	1029	18	0	1029(w)					ρCH_3, νC—C
47	1028	0	0						ρCH_3, νC—C
48	1027	29	0	1017(m)	1018(m)	1018(m)	1020(m)		ρCH_3, Δring
49	950	0	17					944(m)	δC=C=C, ρCH_3
50	948	8	0	950(w)	944(w)	944(w)	944(w)		δC=C=C, ρCH_3
51	930	33	0	932(m)	937(m)	937(m)	938(m)		νC—CH_3, Δring
52	921	0	2						νC—CH_3, Δring
53	783	135	0	787(w)	(*)	(*)	(*)		γCH_α, γNH
54	781	0	2						γCH_α, γNH
55	741	1	0	748(w)					γCH_α, γNH
56	740	0	1						γCH_α, γNH
57	697	2	0						νaN—Cu—N, νC—CH_3
58	685	0	4						νsN—Cu—N, νsO—Cu—O
59	638	51	0	645(m)	648(w)	644(w)	643(w)		γC—CH_3
60	631	0	1						γC—CH_3
61	617	26	0	621(m)	616(w)	616(w)	616(w)		νaO—Cu—O, νaN—Cu—N
62	580	0	7						νsO—Cu—O, νsN—Cu—N
63	545	0	0						γC—CH_3
64	542	0	4					555(w)	γC—CH_3
65	466	49	0	464(vs)	462(s)	462(s)	462(s)		νaO—Cu—O, δC—CH_3
66	451	0	34					466(vs)	νsO—Cu—O, νsN—Cu—N
67	434	11	0	436(m)					Δ
68	403	0	4						Δ
69	338	2	0	337(w)					νaN—Cu—N
70	296	35	0	297(m)					δN—Cu—N, δO—Cu—O

(*continued on next page*)

Table 4 (*continued*)

Theoretical				Experimenta					Assignment
				IR				Raman	
No.	F_s	I_{IR}	A_R	Solid	CH_3CN	$CHCl_3$	CCl_4	Solid	
71	269	0	0						Δ, δC—CH_3
72	260	2	0	276(m)					δC—CH_3
73	256	18	0	259(m)					γN—Cu—N, γO—Cu—O
74	219	0	9					215(s)	νaAPO—Cu—APO
75	197	0	13					192(m)	νsAPO—Cu—APO
76	169	6	0	180(m)					Γring
77	164	0	2						Γring, τCH_3
78	151	0	0						Γring, γC—CH_3
79	142	0	1						Γring
80	113	0	1						τCH_3
81	110	4	0						τCH_3
82	98	0	3						τAPO, τCH_3
83	85	3	0						δAPO
84	41	0	0						τAPO
85	35	2	0						γAPO
86	18	1	1						τCH_3
87	8	1	1						τCH_3

a Fs., theoretical frequency calculated at the UB3LYP/6-311G* level, scaled by 0.9609 and 0.9849 for the 2900–3100 cm^{-1} and below 1700 cm^{-1} regions, respectively. I_{IR}, IR intensity (in kM/mol); and A_R, Raman activity (Å^4/amu), the relative intensities are given in parentheses; v, very; s, strong; m, medium; w, weak; (*), solvent band overlap, ν, stretching; δ, in-plane bending; γ, out-of-plane bending; Δ, in-plane ring deformation; Γ, out-of-plane ring deformation; τ, torsion; ρ, in-plane rocking; π, out-of-plane rocking; i.p., in-phase; o.p., out-of-phase.

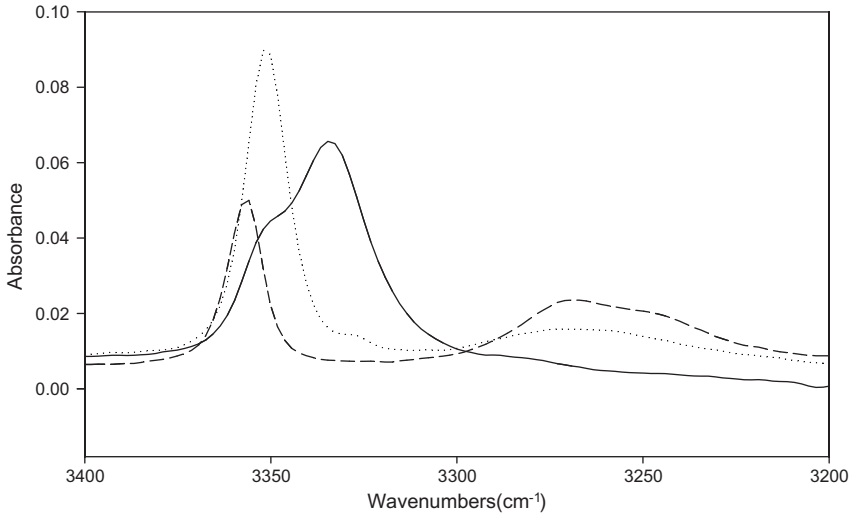

Fig. 8. Infrared spectra of $Cu(APO)_2$ in $CHCl_3$ (...), in CH_3CN (—), and in CCl_4 (- - -).

theoretical results. The best agreement between theoretical and experimental were obtained by using UMPW1PW91/GEN and UB3LYP/6-311G* levels.

The symmetric and asymmetric O—Cu—O and N—Cu—N band frequencies were observed at 464 and 621 cm^{-1}, respectively.

Acknowledgements

We thank the research vice-chancellor at Ferdowsi University of Mashhad for financial support.

Appendix A. Supplementary material

X-ray crystallographic data file (CIF) of $Cu(APO)_2$ and the vibrational frequencies calculated at several theoretical *ab initio* and DFT levels (Table S1) are available from the authors on request.

Supplementary data associated with this article can be found, in the online version, at doi:10.1016/j.molstruc.2010.10.034.

References

[1] E.F. Connor, T.R. Younkin, J.I. Henderson, A.W. Waltman, R.H. Grubbs, Chem. Commun. 9 (2003) 2272.
[2] C.B. Shim, Y.H. Kim, B.Y. Lee, Y. Dong, H. Yun, Organometallics 22 (2003) 4272.
[3] A.A. Elassar, A.A. El-Khair, Tetrahedron 59 (2003) 8463.
[4] C. Kascheres, J. Braz. Chem. Soc. 14 (2003) 945.
[5] G.J.P. Brltovsek, V.C. Gibson, D.F. Wass, Angew. Chem. Int. Ed. 38 (1999) 428.
[6] F. Bao, R. Ma, Y. Jiao, Appl. Organometal. Chem. 20 (2006) 368.
[7] G.E. Gurr, Inorg. Chem. 3 (1964) 614.
[8] M.J. Lacey, Aust. J. Chem. 23 (1970) 841.
[9] PATTY: P.T. Beurskens, G. Admiraal, G. Beurskens, W.P. Bosman, S. Garcia-Granda, R.O. Gould, J.M.M. Smits, C. Smykalla, The DIRDIF program system, Technical Report of the Crystallography Laboratory, University of Nijmegen, The Netherlands, 1992.
[10] DIRDIF99: P.T. Beurskens, G. Admiraal, G. Beurskens, W.P. Bosman, R. de Gelder, R. Israel, J.M.M. Smits, The DIRDIF-99 program system, Technical Report of the Crystallography Laboratory, University of Nijmegen, The Netherlands, 1999.
[11] M.J. Frisch, G.W. Trucks, H.B. Schlegel, G.E. Scuseria, M.A. Robb, J.R. Cheeseman, J.A. Montgomery Jr., T. Vreven, K.N. Kudin, J.C. Burant, J.M. Millam, S.S. Iyengar, J. Tomasi, V. Barone, B. Mennucci, M. Cossi, G. Scalmani, N. Rega, G.A. Petersson, H. Nakatsuji, M. Hada, M. Ehara, K. Toyota, R. Fukuda, J. Hasegawa,

M. Ishida, T. Nakajima, Y. Honda, O. Kitao, H. Nakai, M. Klene, X. Li, J.E. Knox, H.P. Hratchian, J.B. Cross, V. Bakken, C. Adamo, J. Jaramillo, R. Gomperts, R.E. Stratmann, O. Yazyev, A.J. Austin, R. Cammi, C. Pomelli, J.W. Ochterski, P.Y. Ayala, K. Morokuma, G.A. Voth, P. Salvador, J.J. Dannenberg, V.G. Zakrzewski, S. Dapprich, A.D. Daniels, M. C. Strain, O. Farkas, D.K. Malick, A.D. Rabuck, K. Raghavachari, J.B. Foresman, J.V. Ortiz, Q. Cui, A.G. Baboul, S. Clifford, J. Cioslowski, B.B. Stefanov, G. Liu, A. Liashenko, P. Piskorz, I. Komaromi, R.L. Martin, D.J. Fox, T. Keith, M.A. Al-Laham, C.Y. Peng, A. Nanayakkara, M. Challacombe, P.M.W. Gill, B. Johnson, W. Chen, M.W. Wong, C. Gonzalez, J.A. Pople, Gaussian 03, Revision B.03, Gaussian, Inc., Wallingford, CT, 2004. Gaussian 03, Revision B.05, M.J. Frisch, et al. Gaussian, Inc., Pittsburgh, PA, 2003.

[12] A.D. Becke, J. Chem. Phys. 98 (1993) 5648.
[13] C. Lee, W. Yang, R.G. Parr, Phys. Rev. B 37 (1988) 785.
[14] S.F. Tayyari, T. Bakhshi, S.J. Mahdizadeh, S. Mehrani, R.E. Sammelson, J. Mol. Struct. 938 (2009) 76.
[15] C. Adamo, V.J. Barone, J. Chem. Phys. 108 (1998) 664.
[16] GaussView 3.0, Gaussian Inc., Carnegie Office Park, Pittsburgh, PA 15106, USA.
[17] Genplot Package Computer Service, Cornell University, Utica, New York, 1990.
[18] S.F. Tayyari, H. Raissi, F. Tayyari, Spectrochim. Acta 58A (2002) 1681.
[19] Brian C. Smith, Infrared Spectral Intraction: A Systematic Approach, CRC Press, 1999. pp. 135–138.
[20] S.F. Tayyari, T. Bakhshi, M. Ebrahimi, R.E. Sammelson, Spectrochim. Acta 73A (2009) 342.
[21] S.F. Tayyari, R.E. Sammelson, F. Tayyari, H. Rahemi, M. Ebrahimi, J. Mol. Struct. 920 (2009) 301.
[22] S.F. Tayyari, Z. Moosavi-Tekyeh, M. Soltanpour, A. Berenji, R.E. Sammelson, J. Mol. Struct. 892 (2008) 32.
[23] R.E. Sammelson, A. Najafi, M. Azizkhani, F. Lorestani, S.F. Tayyari, J. Mol. Struct. 892 (2008) 32.
[24] S.F. Tayyari, F. Milani-Nejad, Spectrochim. Acta 56A (2000) 2679.
[25] H.F. Holtzclaw Jr., J.P. Collman, R.M. Alire, J. Am. Chem. Soc. 80 (1958) 1100.
[26] H. Junge, H. Musso, Spectrochim. Acta 24A (1968) 1219.
[27] M. Mikami, I. Nakagawa, T. Shimanouchi, Spectrochim. Acta 23A (1967) 1037.
[28] K. Nakamoto, C. Udovich, J. Takemoto, J. Am. Chem. Soc. 92 (1970) 3973.